CHAPTER 3

RESULTS

3.1 Elevation determined by altimeter

Elevations of four hundred and sixty two gravity points in the study area were measured with an altimeter. Flat terrain of less than 40 m elevation is observed in most part of the study area whereas high mountain of 40 to 200 m elevation is observed in the south-east of the study area (Figures 3.1 (a) and 3.1 (b)). Comparison between the elevation determined from the altimeter and topographic map is shown in Figure 3.1c. A good agreement between elevation reading from altimeter and topographic map of 1:50,000 scale is observed by taking account of the altimeter accuracy of 0.5 m and contour interval of topographic map of 10 m and 20 m respectively.

3.2 Density of rock samples

One hundred and eight rock samples were collected from 10 sites in the study area. Locations of sampling points are shown in Figure 3.2 (b). Their measured densities are shown in Table 2.1, and will be used later as constraints in gravity interpretation and modeling.

In Table 3.1, the measured density of Jurassic-Triassic sandstone is 2,560 $\pm$70 kg/m^3, whereas that of Permian limestone is 2,720 $\pm$ 60 kg/m^3. The measured densities of Carboniferous-Devonian-Silurian mudstones are 2,420 $\pm$ 70 kg/m^3 for weathering mudstone and 2,770 $\pm$ 50 kg/m^3 for hard mudstone, whereas that of Triassic granite is 2,620 $\pm$ 70 kg/m^3. The accuracy of density was determined from standard deviation.

It can be observed that hard mudstone of Carboniferous-Devonian-Silurian age is the densest rock but its spatial distribution is limited to some parts of the study area. The densities of Permian limestone, Triassic granite and Jurassic-

Triassic sandstone conform to those determined from southern Thailand (Phethuyluk, 1996, etc.) as shown in Table 3.2.

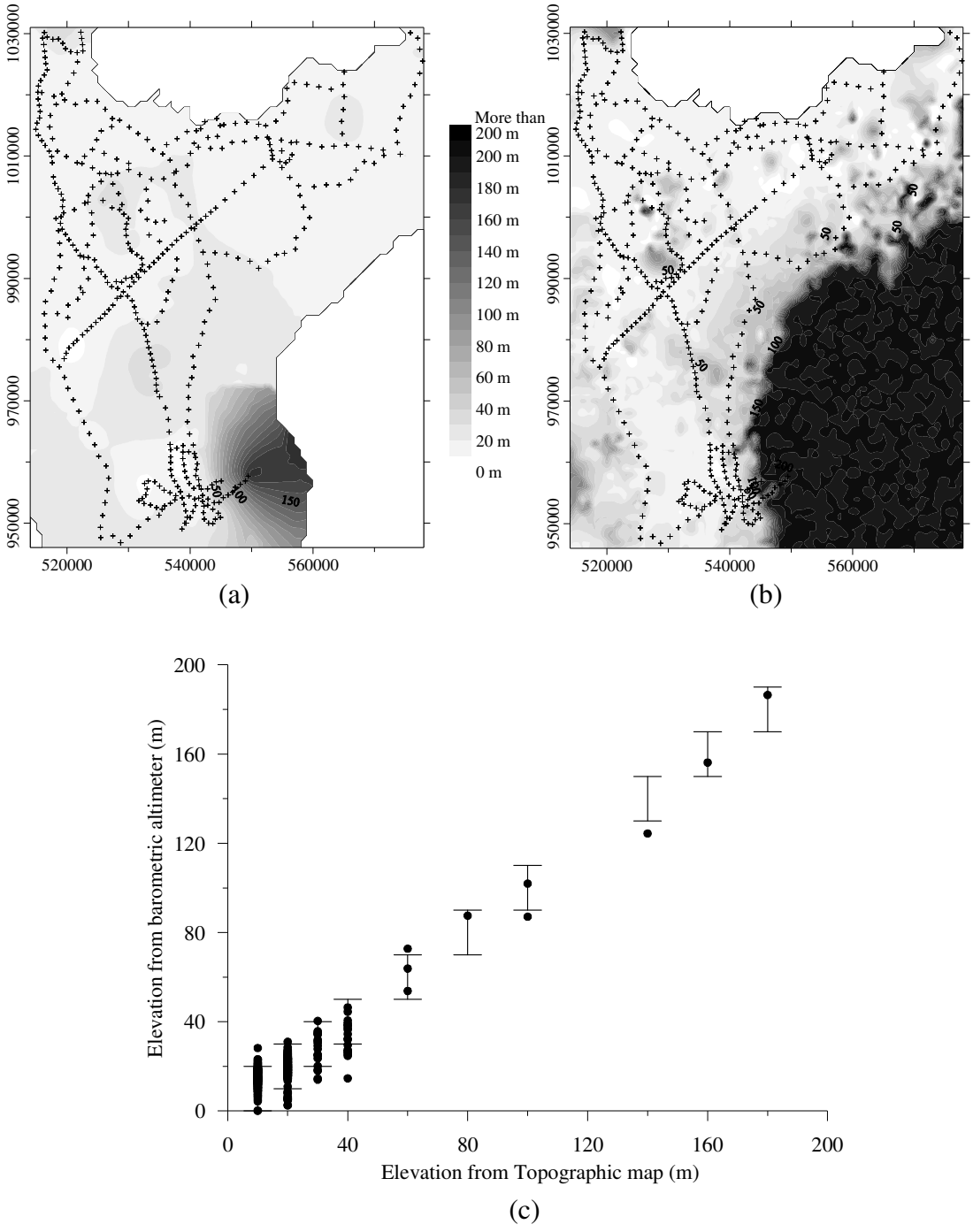

Figure 3.1 The elevation contour maps, (a) data from barometric altimeter measurement, (b) data from topographical map, (a) terrain map of Surat Thani Province of which topography is less than 200 meter above mean sea level.

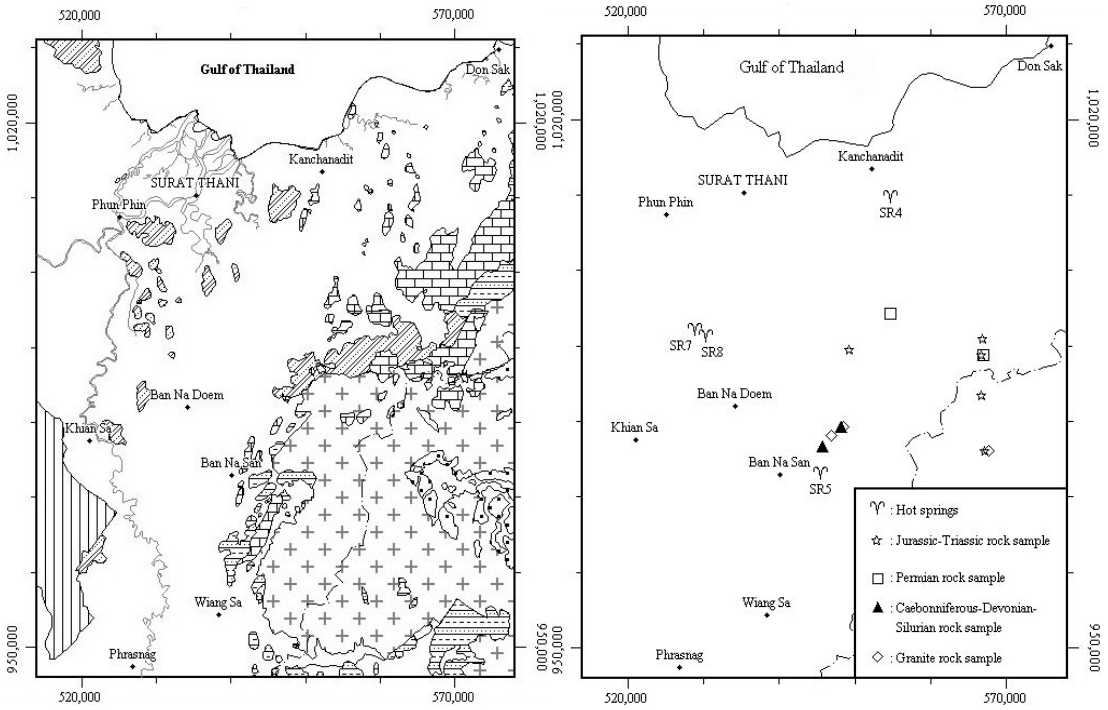

Figure 3.2 (a) Geological map of study area, (b) Locations of each type of rock samples

Table 3.1: Average density of rocks in the study area

Age/Rock type	**Average density (kg/m^3) Range of density**	**Number of sites**	**Number of samples**
Jurassic-Triassic Sandstone	2,560 ± 70 2,390 – 2,640	4	38
Triassic Granite	2,620 ± 70 2,590 – 2,660	3	27
Permian Limestone	2,710 ± 60 2,640 – 2,820	2	28
Carboniferous-Devonian-Silurian Weathering mudstone	2,420 ± 70 2,320 – 2,530	2	10
Hardly mudstone	2,770 ± 50 2,730 – 2,860	1	5

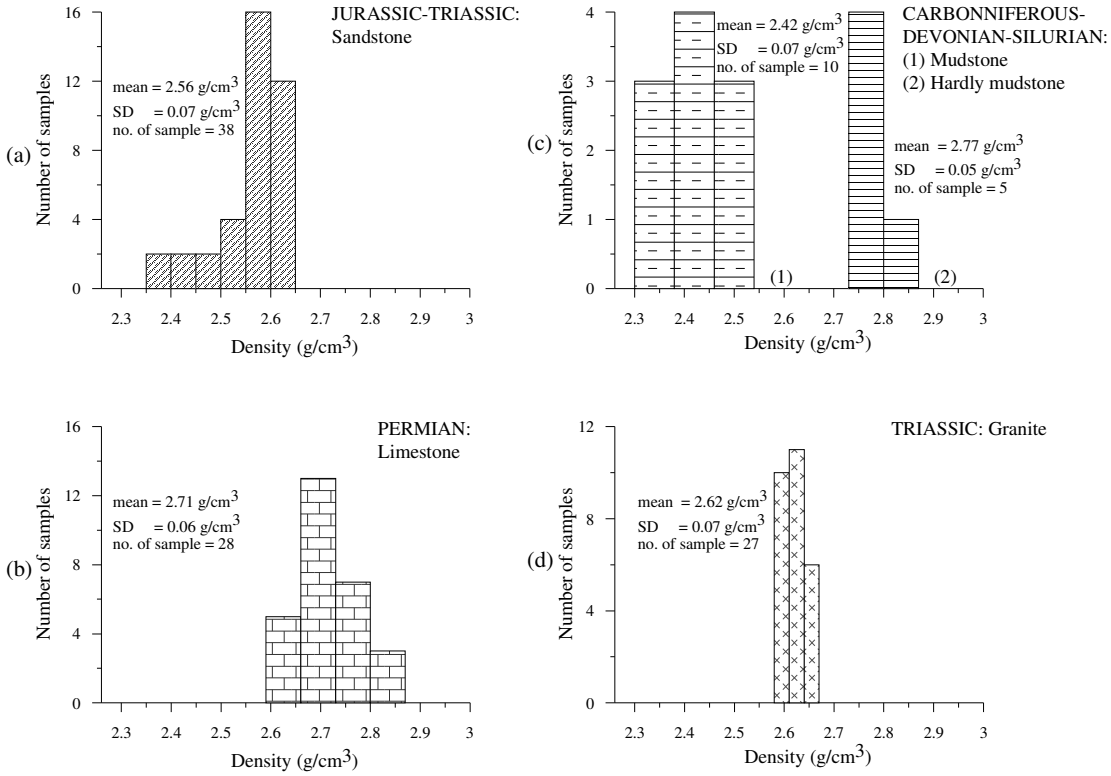

Figure 3.3 Density distributions of rock samples.

Table 3.2: The present and previous study of density on rocks in southern Thailand

Age/Rock type	**Density (kg/m^3)**			
	Range of density			
	Present study	Phethuyluk, 1996	Kaew-on, 1996	Sriapanon, 2000
Jurassic-Triassic	2,560 ± 70	2,250 ± 180	2,560 ± 40	2,420 ± 50
Sandstone	2,390-2,640	1,840-2,710	-	2,400-2,660
Triassic	2,620 ± 70	2,580 ± 60	2,620 ± 40	2,550 ± 70
Granite	2,590-2,660	2,390-2,640	-	2,330-2,660
Permian	2,710 ± 60	2,730 ± 60	2,820 ± 50	-
Limestone	2,640-2,820	2,650-2,820	-	-
Carboniferous-Devonian-Silurian	2,420 ± 70	-	-	-
Weathering mudstone	2,320-2,530	-	-	-
Hardly mudstone	2,770 ± 50	-	-	-
	2,730-2,860	-	-	-

3.3 Bouguer anomaly map of study area

Bouguer anomaly map of the study area is shown in Figure 3.4. From the comparison of the Bouguer anomaly map with the geological and topographic maps (Figures 3.5, 3.6), three distinct areas are categorized as followed;

1. Area of low Bouguer anomaly, -200 g.u. to 150 g.u., is observed on the granitic outcrop in the south-eastern part of the study area. It is a high mountainous area covering Wiang Sra and Ban Na San Distict

2. Area of medium Bouguer anomaly, 150 g.u. to 300 g.u., is observed on Quaternary sediment in the northwestern part of the study area. It is an alluvial plane in Phunphin Distict.

3. Area of high Bouguer anomaly, 300 g.u. to 450 g.u., is observed on Permian limestone, Jurassic sandstone, and Quaternary sediments in the northwest, north and the northeast. It is alluvial plain, upland area, and coastal plain covering Surat Thani and Tha chang District, and parts of Phunphin, Kanchanadit, and Don Sak District.

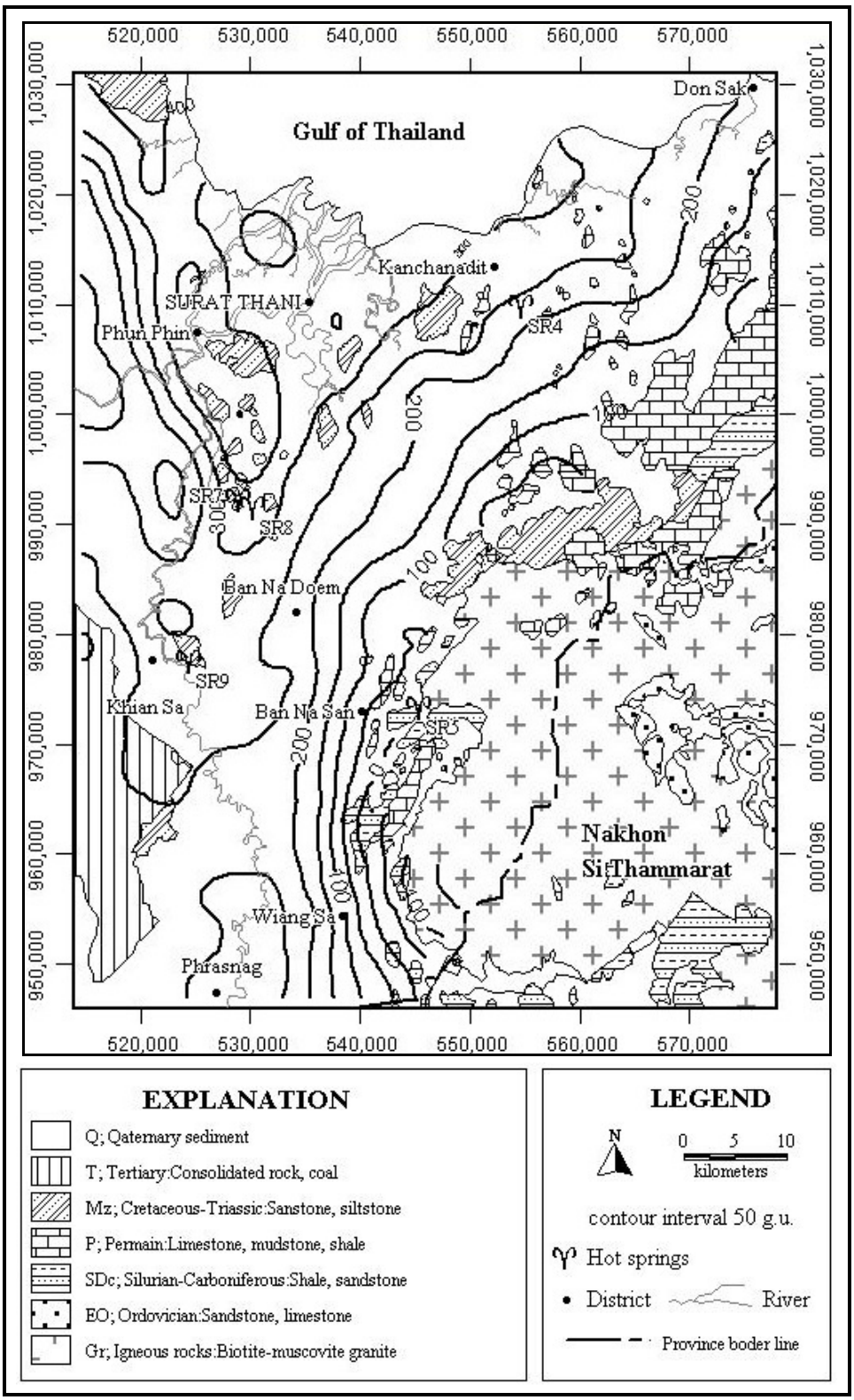

Figure 3.4 Bouguer anomaly superimposed on the geological map of the study area with a contour interval of 50 g.u.

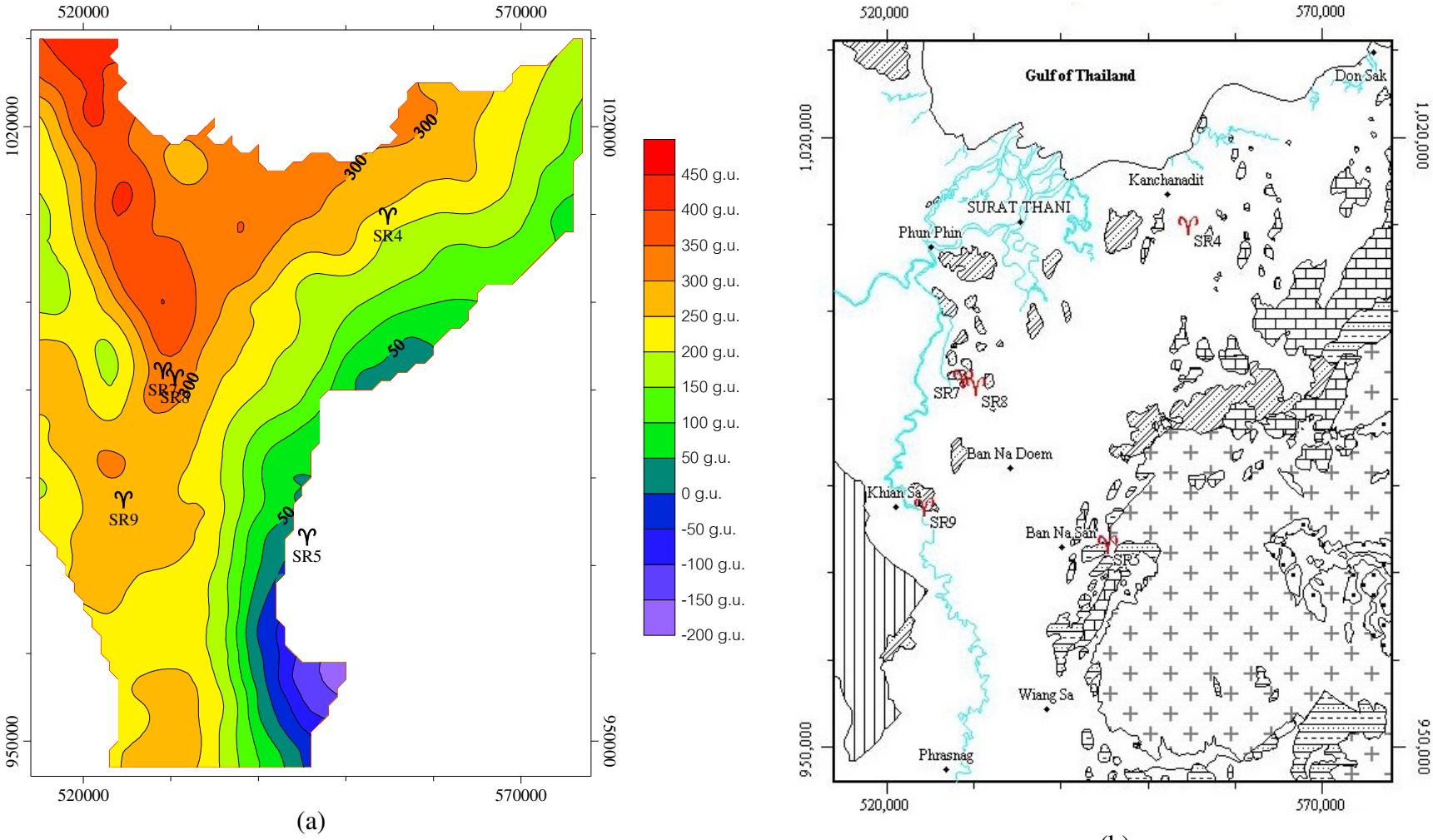

Figure 3.5 (a) Bouguer anomaly map of the study area with a contour interval of 50 g.u. (b) Geological map of the study area.

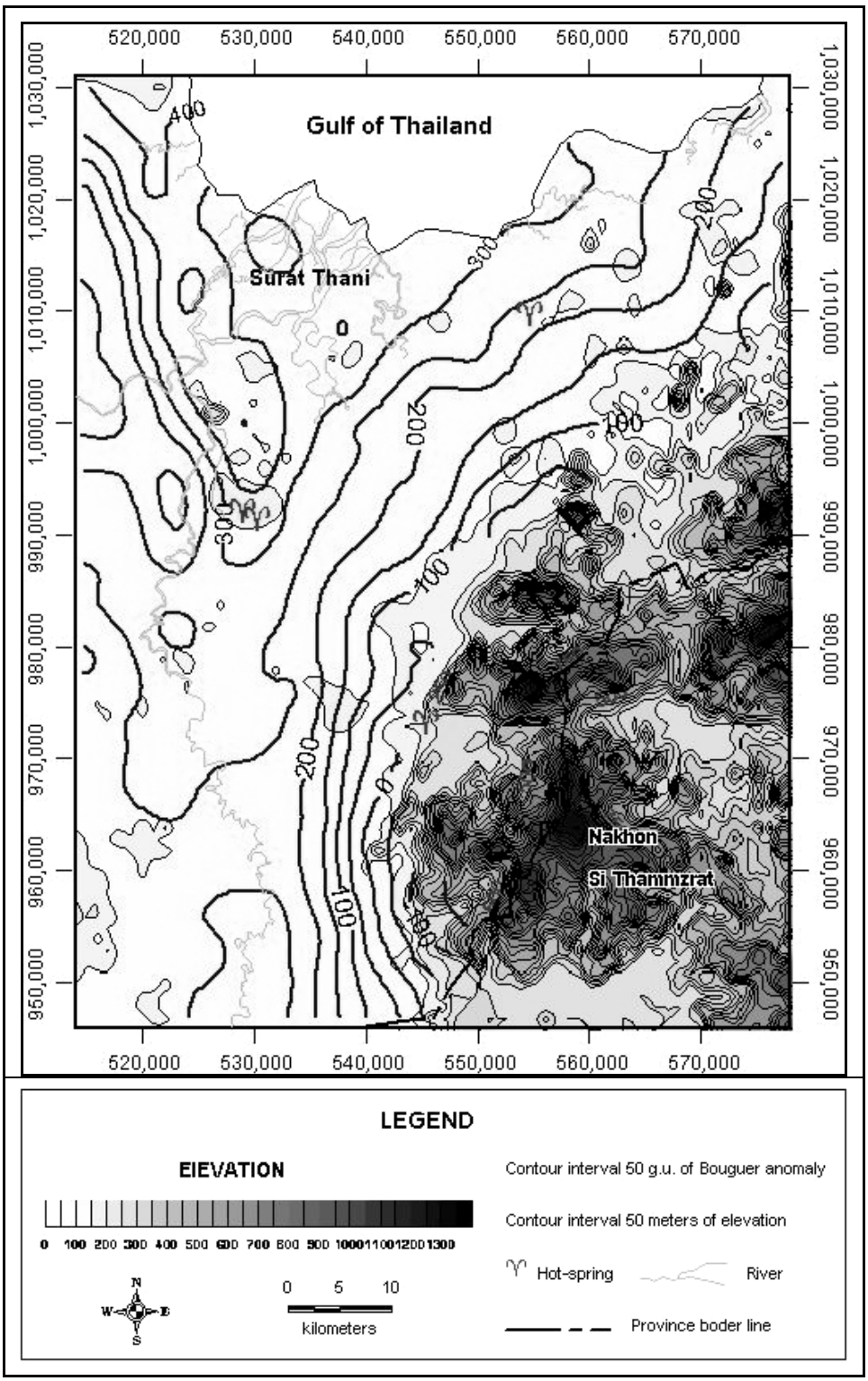

Figure 3.6 Bouguer anomalies superimposed on the elevation map of the study area with a contour interval of 50 g.u.

3.4 Subsurface geological structures

3.4.1 Interpretation of Bouguer anomalies

Seven EW profiles of Bouguer anomaly were selected for gravity modeling to obtain subsurface geological structures of the study area. They are profiles AA' (955000 N), BB' (965000 N), CC' (975000 N), DD' (985000 N), EE' (995000 N), FF' (1005000 N), and GG' (1015000 N) as shown in Figure 3.8.

By considering Bouguer anomaly and geological map of the study area (Figure 3.4 and 3.5 (a)), high Bouguer anomaly is observed on areas covering by Quaternary sediment in the northern part of the study area. Since density of Quaternary sediment is less than other rocks, high density bedrock underlain Quaternary sediment is expected in this area. In contradiction, Bouguer anomaly observed on Kao Luang granite is lower than anomaly observed on sedimentary rocks nearby although density of granite rocks is not much less than density of surrounding sedimentary rocks. It is also expected that high density bedrock would deeply underlain the granitic rock which sequence overlain by sedimentary rocks and Quaternary sediment.

Talong et al. (2001) reported that the course of the Tapee River and also parts of the Phum Duang River seemed to be influenced by vertical tectonic movements (Figure 1.11). It is, therefore, possible that normal faults are effective for the geology structure of study area. Harrison et al. (1997) also reported that the dolomite and dolomitic limestone in Surat Thani is in Um Luk Formation of Ratburi Group. The density of this limestone is 2,700 to 2,850 kg/m^3. It is possible that this limestone underlies younger sedimentary rocks and sediment in area of high Bouguer anomaly.

Keaw-on (1996) and Phethuayluk (1996) also observed low Bouguer anomaly on granitic rock and high Bouguer anomaly on sedimentary rocks in Satun, Songkhla, Phattalung, and Trang Provinces, areas south of the present study area. Their interpreted subsurface geological model was granite of density 2,620 kg/m^3 and more than 10 kilometers thick overlying bedrock of density 2,800 kg/m^3.

The granitic rock in southern Thailand belongs to Central Belt Granite (Putthapiban, 2002). It was convinced that granite was originated from melting rock at depth in Triassic to Jurassic Age when Shan-Thai Terrance collided with Indochina Terrance (Bunopas, 1981, Moores and Fairbridge, 1997, and Kaew-on, 1996). Therefore, it is possible to assume that granitic rock in the present study area was formed by crust melting and being pushed up to surface as "Granitic plume" (Figure 3.7).

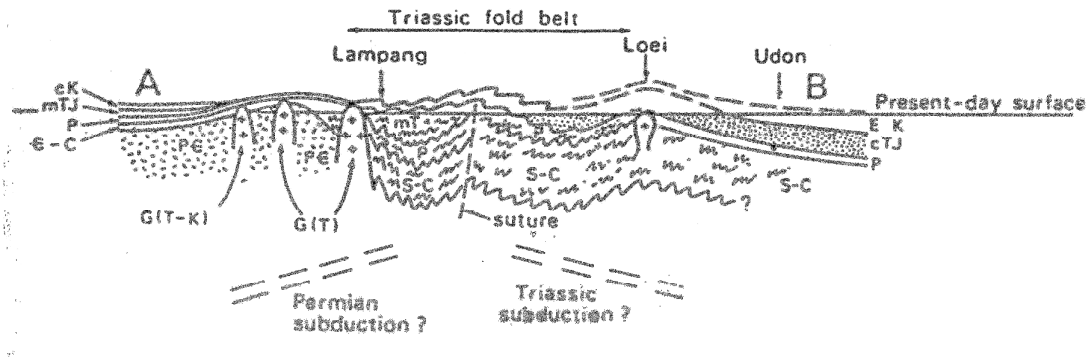

Figure 3.7 The forming of granitic plume when Shan-Thai terrance collided with Indochina terrance (taken from Moores and Fairbridge, 1997)

In order to decrease the degree of ambiguity in the gravity modeling of the subsurface geological structures of the study area, information on rock densities, surface geology, available geological sections and shallow earth models obtained from resistivity sounding measurement were used as constraints in the modeling. In the present study, the densities of 2,710 kg/m^3; 2,770 kg/m^3; 2,560 kg/m^3; and 2,100 kg/m^3 were assigned for Permian limestone, Silurian-Devonian-Carboniferous rock, Cretaceous-Triassic rocks and Quaternary sediments respectively in gravity modeling.

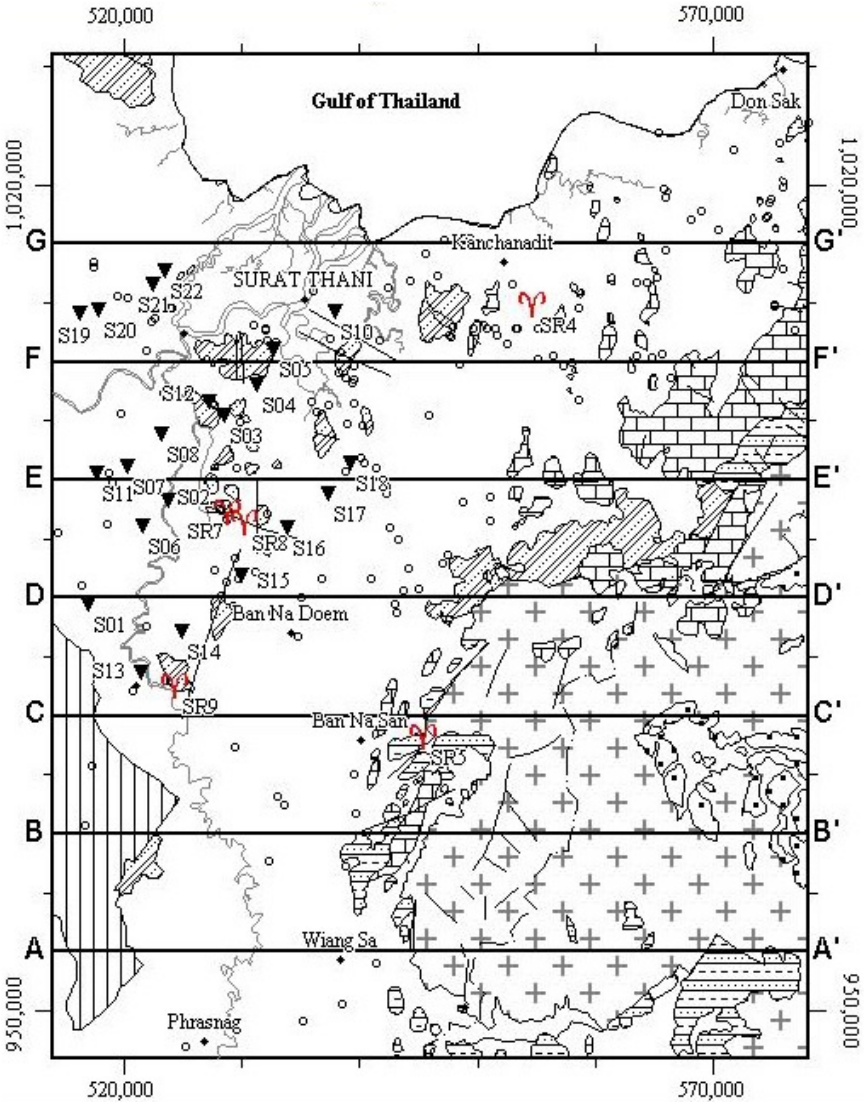

Figure 3.8 Locations of gravity profiles, vertical resistivity sounding points (triangle), and available groundwater wells (circle) on geological map of the study area.

3.4.1.1 Profile AA´ (955000N)

Gravity anomaly and subsurface geological model of the profile AA' are shown in Figure 3.9. A gentle increase of Bouguer anomaly from about 250 g.u. on the western part of the profile to 270 g.u. at 530000E followed by a strong decrease of anomaly from 270 g.u. to -150 g.u. on the eastern end of the profile was clearly observed (Figure 3.9 (a)).

In gravity modeling, Carboniferous rock and underlying rocks were assigned as basement rock. Granite of about 13 km thick was modeled to explain low Bouguer anomaly on the eastern end of the profile (Figure 3.9 (b)). Permian limestone of 60 to 560 m thick overlying basement rock and in-turn underlying Triassic-Jurassic rocks of 150 to 300 m thick were modeled to explain Bouguer anomaly along the profile. In addition, Quaternary sediment of 40 to 300 m thick at the very shallow depth between 516500E to 539700E was modeled in order to follow surface geology of the study along the profile. A step change in the thickness of Quaternary sediment was observed at 520000E to 532000E below the Tapee River.

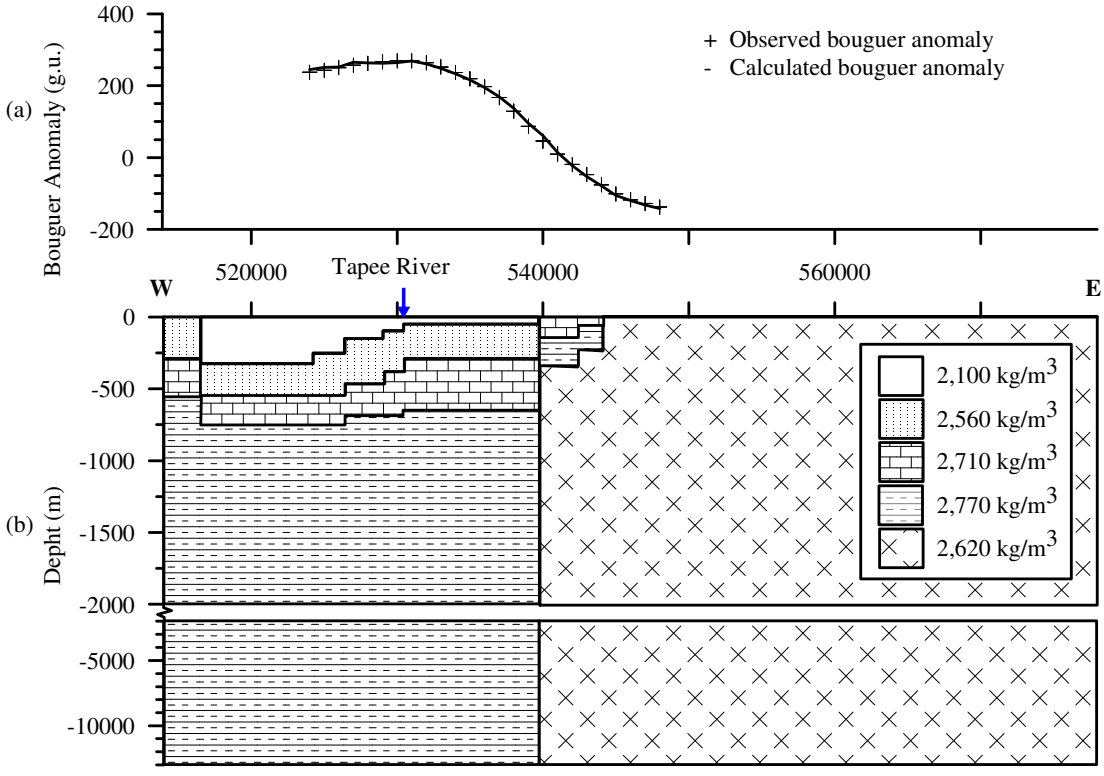

Figure 3.9 (a) Observed and calculated Bouguer anomalies, (b) geological model obtained from gravity interpretation on profile AA´

3.4.1.2 Profile BB´ (965000N)

Gravity anomaly and subsurface geological model of the profile BB' are shown in Figure 3.10. A gentle increase of the Bouguer anomaly from about 230 g.u. on the western end of the profile to 250 g.u. at 523000E, followed by a gentle decrease of anomaly to 200 g.u. at 535000E and a strong decrease to -30 g.u. on the eastern end of the profile was clearly observed (Figure 3.10 (a)).

In gravity modeling, Carboniferous rock and underlying rocks were assigned as basement rock. Similar with profile AA', granite of about 13 km thick was modeled to explain low Bouguer anomaly on the eastern end of the profile (Figure 3.10 (b)). Permian limestone of 50 to 350 m thick overlying basement rock and in-turn underlying Triassic-Jurassic rocks of 350 to 600 m thick was modeled to explain Bouguer anomaly along the profile. In addition, Quaternary sediment of 30 to 350 m thick was modeled on at the very shallow depth between 515500E to 535000E in order to follow surface geology of the study along the profile. A step change in the thickness of Quaternary sediment was observed at 525000E to 535000E below the Tapee River.

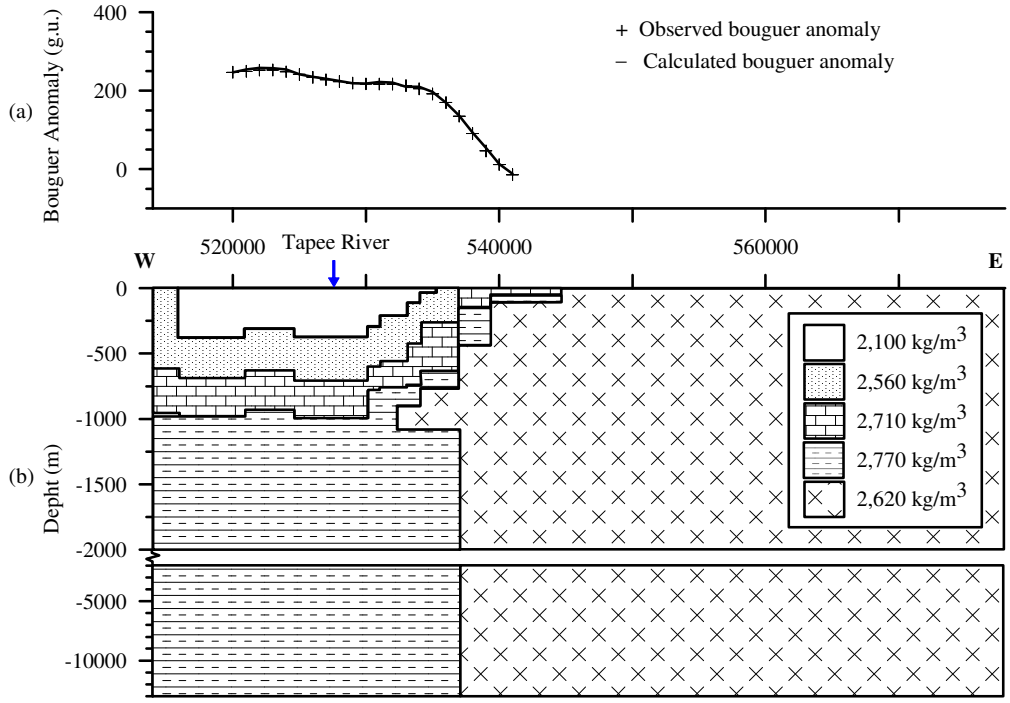

Figure 3.10 (a) Observed and calculated Bouguer anomalies, (b) geological model obtained from gravity interpretation on profile BB´

3.4.1.3 Profile CC´ (975000N)

Gravity anomaly and subsurface geological model of the profile CC' are shown in Figure 3.11. An increase of the Bouguer anomaly from about 210 g.u. on the western end of the profile to 270 g.u. at 522000E, followed by a gentle decrease of anomaly to 250 g.u. at 534000E, and then followed by a strong decrease to 40 g.u. on the eastern end of the profile was clearly observed (Figure 3.11 (a)).

In gravity modeling, Carboniferous rock and underlying rocks were assigned as basement rock. Similarly, Granite of about 13 km thick was modeled to explain low Bouguer anomaly on the eastern end of the profile (Figure 3.11 (b)). Permian limestone of 170 to 800 m thick overlying basement rock, and in-turn underlying Triassic-Jurassic rocks of 100 to 600 m thick was modeled to explain Bouguer anomaly along the profile. In addition, Quaternary sediment of 60 to 330 m thick was modeled on at the very shallow depth between 514000E to 541500E to follow surface geology of the study along the profile. A step change in the thickness of Quaternary sediment was observed at 514000E to 530000E below the Tapee River.

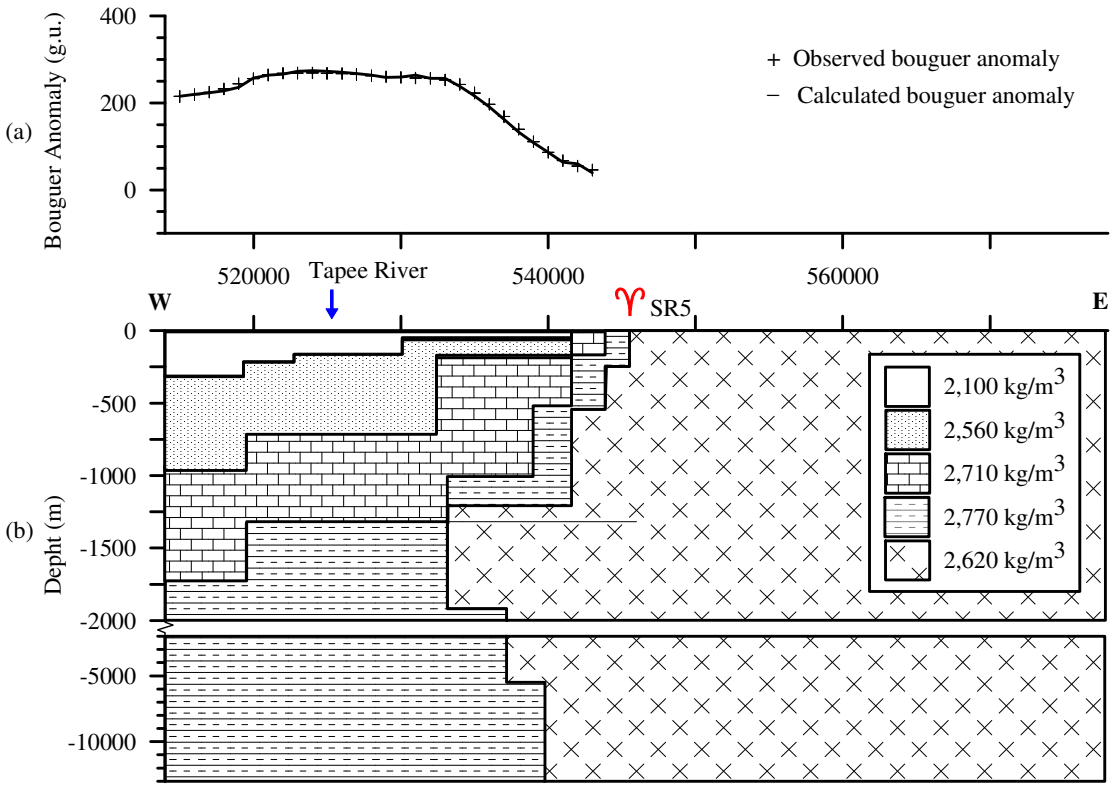

Figure 3.11 (a) Observed and calculated Bouguer anomalies, (b) geological model obtained from gravity interpretation on profile CC´

3.4.1.4 Profile DD´ (985000N)

Gravity anomaly and subsurface geological model of the profile DD' are shown in Figure 3.12. An increase of the Bouguer anomaly from about 250 g.u. on the western part of the profile to 290 g.u. at 520000E, followed by a gentle decrease of anomaly to 260 g.u. at 524000E, a gentle increase to 290 g.u. at 528000E, and then followed by a strong decrease to 70 g.u. on the eastern end of the profile were observed (Figure 3.12 (a)).

In gravity modeling, Carboniferous rock and underlying rocks were assigned as basement rock. Granite of about 5,500 m thick was modeled to explain low Bouguer anomaly on the eastern end of the profile (Figure 3.12 (b)). Permian limestone of 190 to 490 m thick overlying basement rock, and in-turn underlying Triassic-Jurassic rocks of 110 to 650 m thick was modeled to explain Bouguer anomaly along the profile. Quaternary sediment of 80 to 280 m thick was modeled at the very shallow depth between 514000E to 546000E to follow surface geology of the study area along the profile. A step change in the thickness of Quaternary sediment was observed at 526000E to 530600E below the Tapee River.

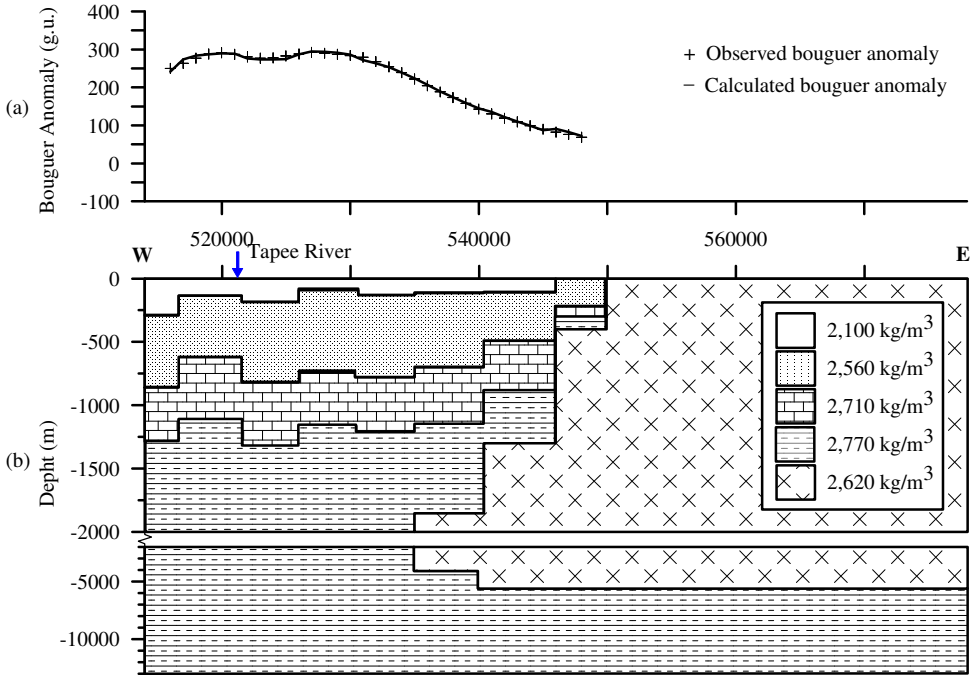

Figure 3.12 (a) Observed and calculated Bouguer anomalies, (b) geological model obtained from gravity interpretation on profile DD´

3.4.1.5 Profile EE´ (995000N)

Gravity anomaly and subsurface geological model of the profile EE' are shown in Figure 3.13. A decrease of the Bouguer anomaly from 260 g.u. on the western end of the profile to 190 g.u. at 523000E, followed by a strong increase to 370 g.u. at 530000E, and then followed by a strong decrease to 40 g.u. on the eastern end of the profile was observed (Figure 3.13 (a)).

In gravity modeling, Carboniferous rock and underlying rocks were assigned as basement rock. Granite of about 13 km thick was modeled to explain low Bouguer anomaly on the eastern end of the profile (Figure 3.13 (b)). Permian limestone of 500 to 1600 m thick overlying basement rock, and in-turn underlying Triassic-Jurassic rocks of 150 to 440 m thick was modeled to explain Bouguer anomaly along the profile. In addition, Permian dolomitic limestone (2,840 kg/m^3) of 280 m thick overlying Permian limestone was modeled to explain very high anomaly around SR7 and SR8 hot springs. Moreover, Quaternary sediment the 60 to 100 m thick was modeled on the very shallow depth along the profile. A step change in thickness of Quaternary sediment was observed at 517000E to 527000E below the Tapee River.

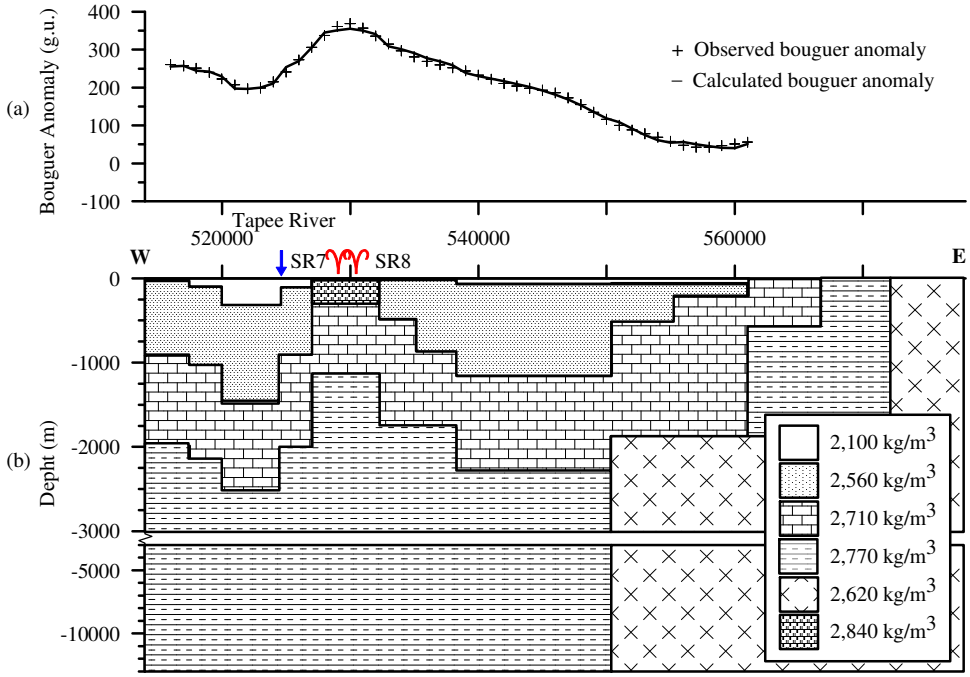

Figure 3.13 (a) Observed and calculated Bouguer anomalies, (b) geological model obtained from gravity interpretation on profile EE´

3.4.1.6 Profile FF′ (1005000N)

Gravity anomaly and subsurface geological model of the profile FF' are shown in Figure 3.14. A strong increase of Bouguer anomaly from about 200 g.u. on the western end of the profile to 370 g.u. at 525000E followed by a gentle decrease to 130 g.u. on the eastern end of the profile was observed (Figure 3.14 (a)).

In gravity modeling, Carboniferous rock and underlying rocks were assigned as basement rock. Granite of about 3 km thick extending from 544200E to 578000E was modeled to explain low Bouguer anomaly on the eastern end of the profile (Figure 3.14 (b)). Permian limestone of 800 to 1600 m thick overlying basement rocks, and in-turn underlying Triassic-Jurassic rocks of 30 to 830 m thick was modeled to explain Bouguer anomaly along the profile. Similar to profile EE', Permian dolomitic limestone of about 380 m overlying Permian limestone was modeled to explain very high anomaly at 525000E. In addition, Quaternary sediment of 30 to 400 m thick was modeled on at the surface along the profile in order to follow surface geology of the study along profile, except areas from 529200E to 532500E and from 547000E to 552200E where Triassic-Jurassic rocks and/or Permian limestone expose at the surface. A step change in thickness of Quaternary sediment was observed at 514000E to 523000E below the Tapee River.

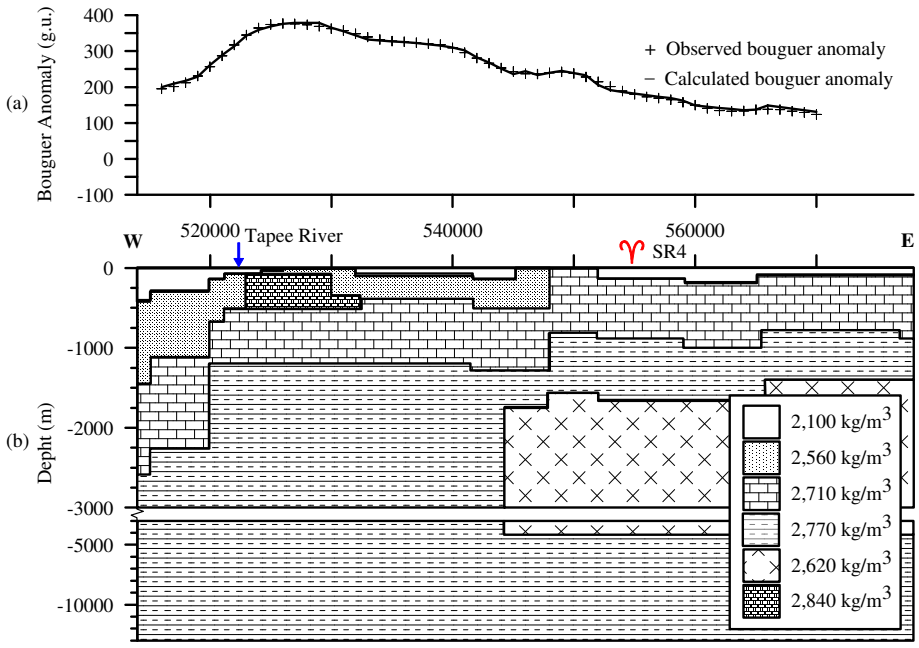

Figure 3.14 (a) Observed and calculated Bouguer anomalies, (b) geological model obtained from gravity interpretation on profile FF′

3.4.1.7 Profile GG´ (1015000N)

Gravity anomaly and subsurface geological model of the profile GG' are shown in Figure 3.15. A strong increase of Bouguer anomaly from about 210 g.u. on the western end of the profile to 380 g.u. at 525000E, followed by a strong decrease to 280 g.u. at 530000E, remains constant between 530000E and 545000E, and followed by a gentle decrease to 250 g.u. at 565000E and then a strong decrease to 150 g.u. on the eastern end of the profile was observed (Figure 3.15 (a)).

In gravity modeling, Carboniferous rock and underlying rocks were assigned as basement rock. Granites of about 1,000 m thick from 550000E to 570000E and of about 4,000 m thick from 570000E to 580000E were modeled to explain low Bouguer anomaly on the eastern end of the profile (Figure 3.15 (b)). Permian limestone of 750 to 1350 m thick overlying basement rock, and in-turn underlying Triassic-Jurassic rocks of 200 to 550 m thick was modeled to explain Bouguer anomaly along the profile. Similar to profile FF', Permian dolomitic limestone of about 1800 m thick overlying Permian limestone was modeled to explain very high anomaly at 525000E. In addition, Quaternary sediment of 30 to 240 m thick was modeled near the surface from between 514000E to 571000E and from 514000E to 526000E in order to follow surface geology along the profile.

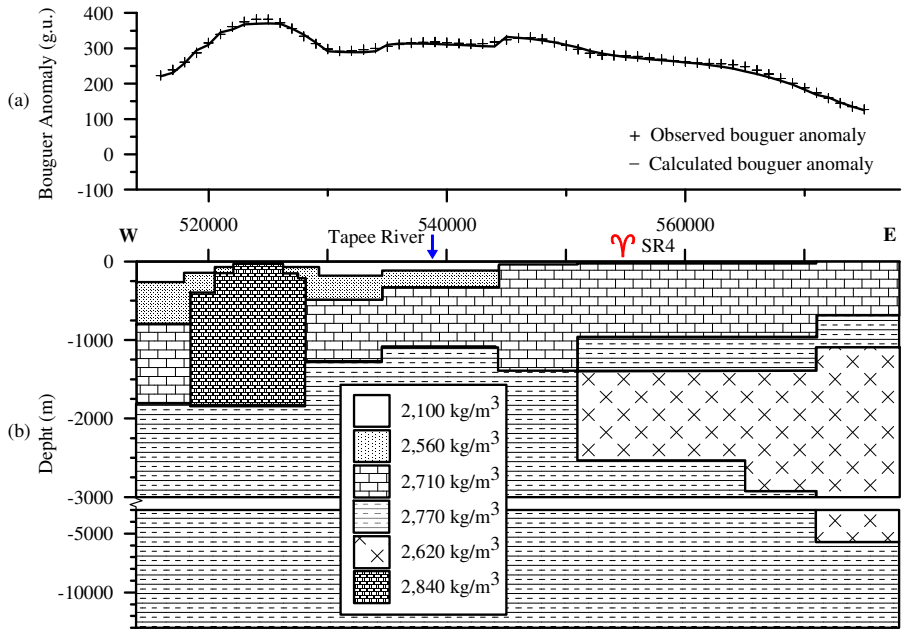

Figure 3.15 (a) Observed and calculated Bouguer anomalies, (b) geological model obtained from gravity interpretation on profile GG´

3.4.2 The interpretation of vertical electrical sounding (VES)

Since high Bouguer anomaly strip trending NW-SE was observed on hot-spring areas, SR7 in Phun Phin District and SR8 in Ban Na Doem District, high density rock at very shallow depth is expected in these areas. The vertical electrical soundings (VES) with Schlumberger electrode configuration were also conducted in this study to determine depth and to delineate boundaries of this high density rock. They will be used as constraints in gravity modeling. According to gravity modeling in section 3.4.1, Permian dolomitic limestone and Permian limestone were modeled as causative bodies of this high gravity anomaly. All together twenty one sounding points were placed on four profiles perpendicular to this high anomaly strip (Figures 3.16 (a) and 3.16 (b)).

In general, the sounding curves obtained from the present study are of bowl-type shape, representing approximately 3-layer earth model of which resistivity of the middle layer is less than those above and below. Sounding results are shown in three groups according to their locations relative to the NW-SE strip of high Bouguer anomaly (Figure 3.16 (c)). The west group which is to the west of this high anomaly strip consists of sounding points S01, S02, S05, S07, S08, S11, S13, S14, S19, and S20. The central group which is on the high anomaly strip comprises sounding points S03, S04, S12, S15, S16, S21, and S22. The east group which is to the east of this high anomaly strip consists of sounding points S06, S10, S17, and S18.

Sounding curves of the west group, the central group, and the east group are shown in Figures 3.17, 3.18 and 3.19 respectively. Their interpreted model parameters are shown in Table 3.3, 3.4, and 3.5 respectively.

In case of the west group, no high resistive bedrock was reached. In this group, the bottom layer of low resistivity, about 10 to 60 ohm-m, underlies the top layer of variable resistivity, 100 to 500 ohm-m.

For the central group, high resistive bedrock, about 600 to 1,000 ohm-m, was reached at depths 75 to 195 m except at sounding point S22. This high resistive bedrock underlies the middle layer of low very low resistivity, about 7 to 23 ohm-m which subsequently underlies the top layer of variable resistivity, 100 to 2,000 ohm-m.

Similar to the central group, high resistive bedrock of about 900 ohm-m was reached for the eastern group but at a greater depth, about 160 to 280 m. This high resistive bedrock underlies the middle layer of low resistivity, about 9 to 33 ohm-m, and subsequently overlain by the top layer of variable resistivity, about 70 to 1,100 ohm-m.

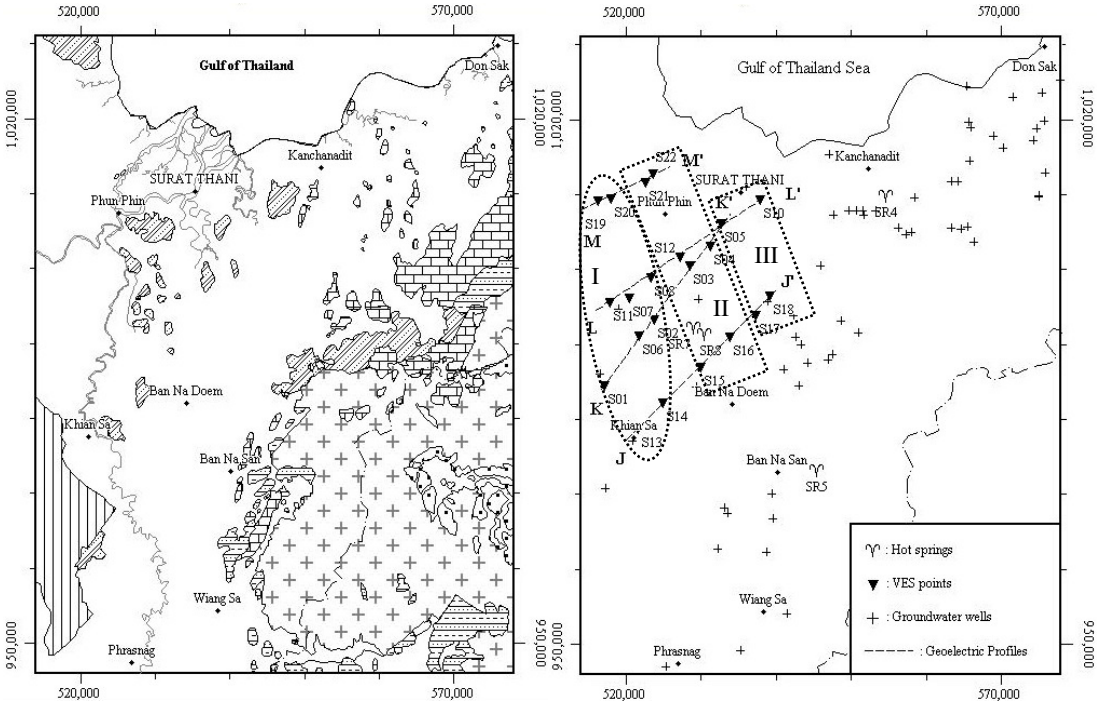

Figure 3.16 (a) Bouguer anomaly superimposed on geological map, (b) Locations of sounding points, groundwater wells, geoelectric profiles, and groups of sounding points (I, II, and III represent the west group, the central group, and the east group respectively).

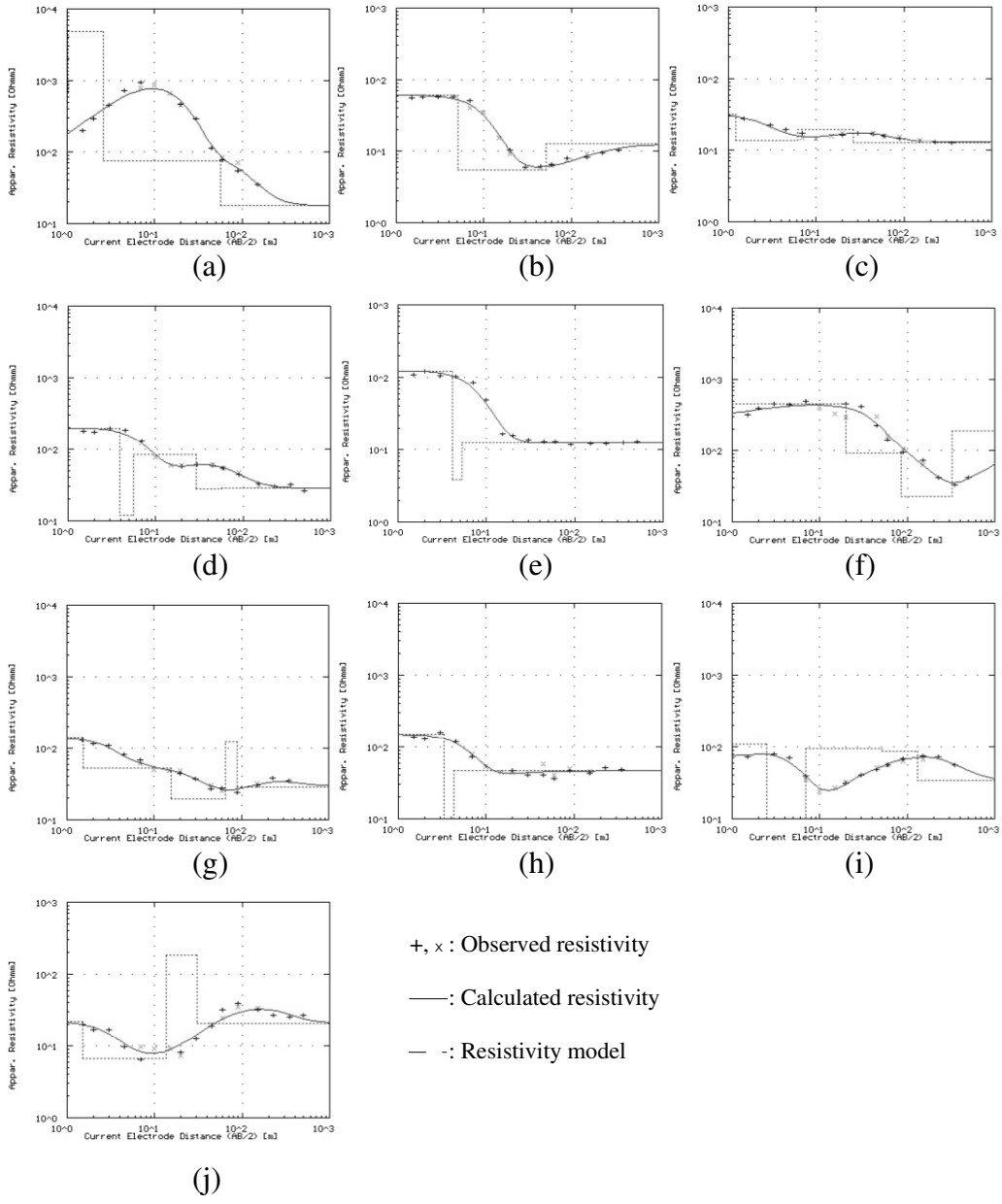

Figure 3.17 The sounding curves of the west group; (a) S01, (b) S02, (c) S06, (d) S07, (e) S08, (f) S11, (g) S13, (h) S14, (i) S19, and (j) S20.

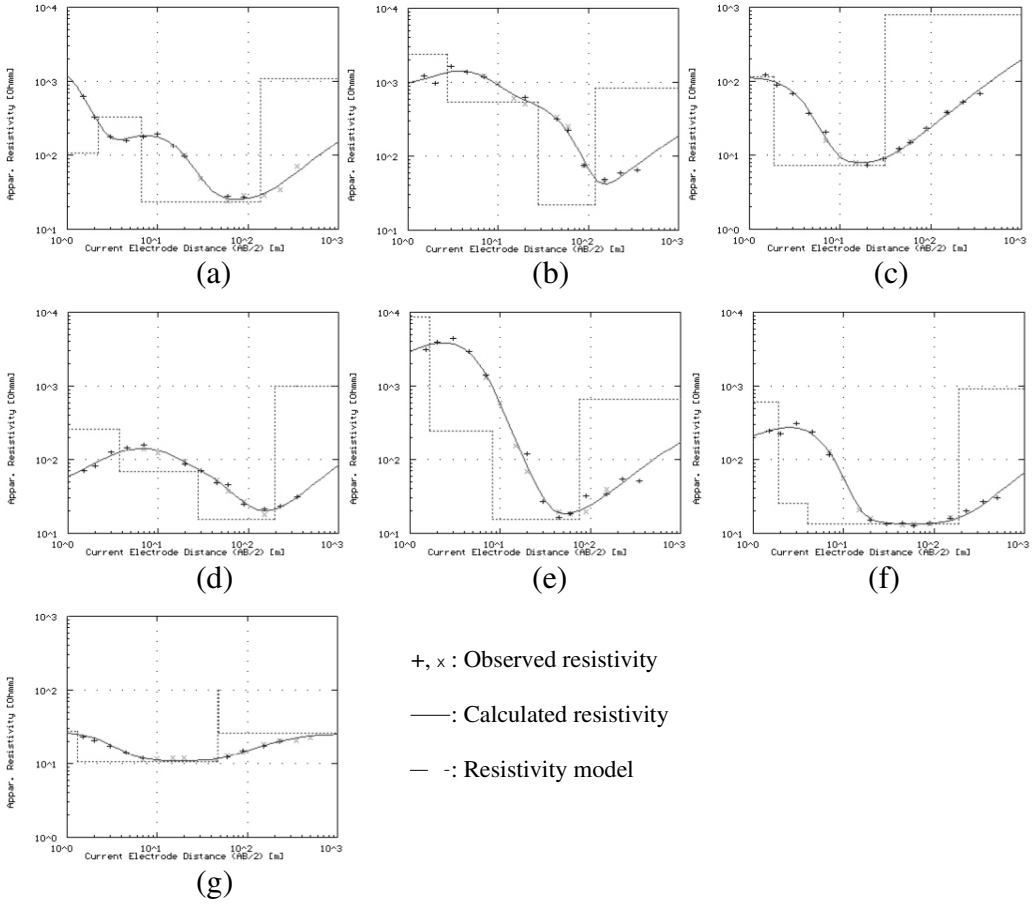

Figure 3.18 The sounding curves of the central group; (a) S03, (b) S04, (c) S12, (d) S15, (e) S16, (f) S21, and (g) S22.

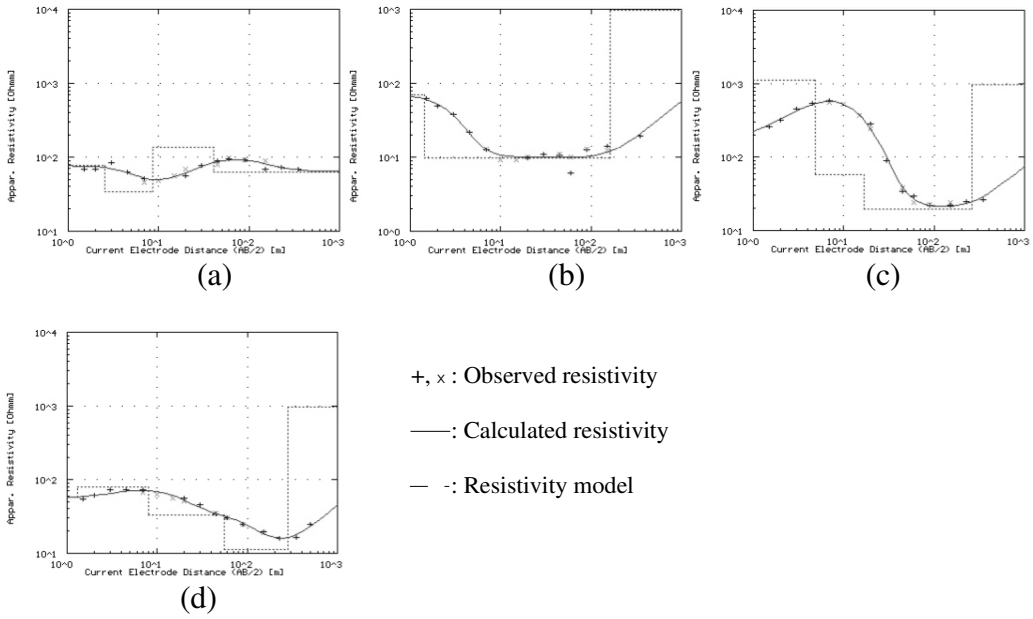

Figure 3.19 The sounding curves of the east group; (a) S05, (b) S10, (c) S17, and (d) S18.

Table 3.3: The interpreted resistivity model of sounding points of different groups

Group	St.	Layer 1		Layer 2		Layer 3		Layer 4		Layer 5		Layer 6	
		Resistivity	Depth	Resistivity	Depth	Resistivity	Depth	Resistivity	Depth	Resistivity	Depth	Resistivity	Depth
West	S01	104	0	667	0.5	4889	1.0	76	2.6	18	57.2	-	-
	S02	61	0	5	5.1	13	51.3	-	-	-	-	-	-
	S05	77	0	34	2.5	136	8.7	63	40.1	-	-	-	-
	S07	197	0	12	1.2	83	5.6	28	28.9	28	57.1	-	-
	S08	122	0	4	4.1	12	5.3	-	-	-	-	-	-
	S11	316	0	451	0.7	91	20.0	23	85.6	187	322.0	-	-
	S13	143	0	52	1.5	20	15.4	121	65.9	29	89.7	-	-
	S14	149	0	10	3.3	46	4.3	-	-	-	-	-	-
	S19	71	0	110	0.8	10	2.5	93	6.9	85	51.0	34	131.5
	S20	22	0	7	1.5	182	13.6	21	30.6				
Central	S03	2129	0	106	0.6	330	2.3	23	6.7	1079	137.1	-	-
	S04	864	0	2383	0.8	536	2.7	22	27.9	850	117.8	-	-
	S12	116	0	7	1.9	801	30.9	-	-	-	-	-	-
	S15	46	0	262	0.7	68	3.7	16	27.9	995	194.9	-	-
	S16	1928	0	8558	0.5	250	1.7	16	8.2	672	75.4	-	-
	S21	172	0	604	0.7	26	1.9	13	4.0	912	186.1	-	-
	S22	27	0	11	1.3	100	45.6	26	1.0	-	-	-	-
East	S06	32	0	14	1.2	20	6.2	13	26.3	-	-	-	-
	S10	71	0	10	1.4	959	161.6	-	-	-	-	-	-
	S17	189	0	1110	0.9	57	4.9	20	16.6	981	262.1	-	-
	S18	57	0	79	1.3	33	8	11	55.4	970	279.7	-	-

3.4.3 Comparison of resistivity model with available geological log

The information of geological from drilling holes in the study area is obtained from Department of Ground Water Resources. Though there are numbers of groundwater wells in study area, but only one of them, "well no. 6753", reaches limestone bedrock at 152 m depth. This well is in vicinity of sounding point "S10". A comparison between the resistivity model of S10 and the geological log of well no. 6753 is shown in Figure 3.20. It can be observed that the high resistive bottom layer, 958.9 ohm-m at the depth of 160 m, corresponds with the limestone bedrock at the depth of 156 m and the middle layer of very low resistivity, 9.8 ohm-m of about 160 m thick, corresponds with clay layer of 156 m thick which overlies the limestone bedrock.

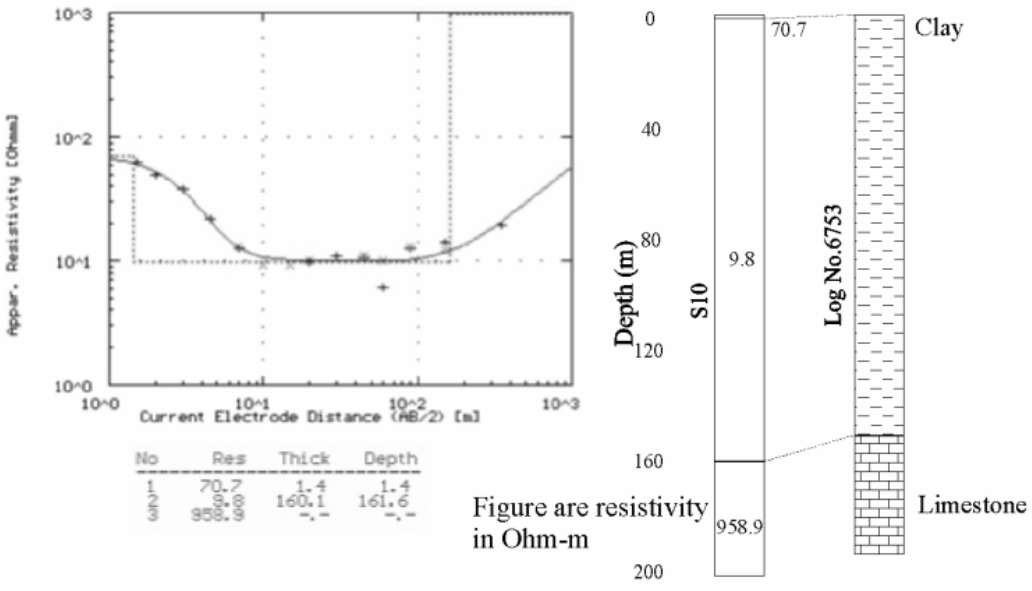

Figure 3.20 A comparison between resistivity model of sounding point S10 and geological log of groundwater well no. 6753 in the study area.

3.4.4 Depth slices of interpreted resistivity model

Depth slices of the interpreted resistivity model of the study area at 0 m, 50 m, 100 m, 150 m, 200 m and 250 m are shown in Figure 3.21. It can be observed clearly that two hot springs, SR7 and SR8, are located on the western boundary of a high resistive band, higher than 600 ohm-m, trending approximately N36W in the central part of the study area.

The resistive band extends vertically from 1.5 m to 250 m. At a shallow depth of 1.5 m, it appears as a continuous band of about 10 km x 10 km. This band of high resistivity appears as single point and two separated points of high resistivity at depths of 50 m and 100 m respectively. At a depth of 150 m, a band of high resistivity is observed again. However, this band of high resistivity is separated into 2 units which are shifted in NE-SW direction at depths of 200 m and 250 m. In addition, a high resistive zone is also observed in the northeastern part of the study area.

It is likely that the high resistive band is bounded by two NW-SE normal faults as proposed in Figure 3.21. In addition, a NE-SW strike-slip fault may cause a NE-SW shift of 2 high resistive units at depths of 200 m and 250m (Figures 3.21 (b1) and (b2)). The locations of these proposed faults on the Bouguer anomaly map and the depth map of Permian limestone in the study area is shown in Figures 3.21 (b1) and 3.21 (b2) respectively. It can be seen clearly that the NW-SE band of high Bouguer anomaly and a NW-SE uplift of Permian limestone are bounded by these faults. Moreover, it is observed those two hot springs, SR7 and SR8, are located exactly at the crossed region of these faults. This probably indicates that NW-SE and NE-SW faults in the study area play important role as pathways of hot water for hot spring in this study area.

Comparisons between depth slices of resistivity model in color shaded maps with the contour maps of Bouguer anomaly within the study area are shown in Figure 3.22. It can be observed that other hot pings, SR4, SR5 and SR9, align themselves along the extensions of the proposed NW-SE and NE-SW faults which bound the high resistive band or the uplife of Permian limestone.

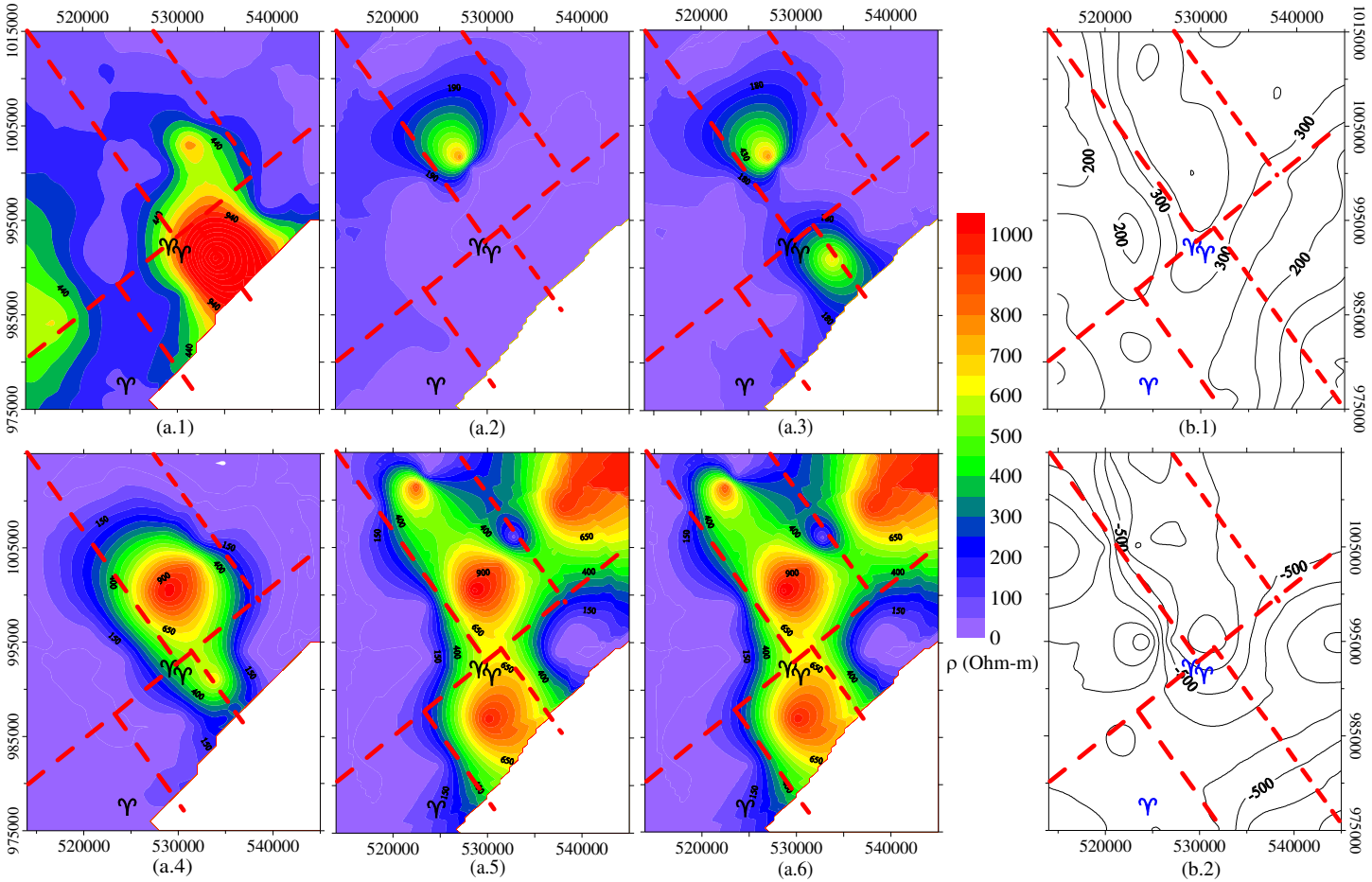

Figure 3.21 Contour maps of resistivity modeled at difference penetration depths around SR7 and SR8 hot-spring (a.1) 1.5 m., (a.2) 50 m., (a.3) 100 m., (a.4) 150 m., (a.5) 200 m., (a.6) 250 m. (b.1) Bouguer anomaly map with a contour interval of 50 g.u. (b.2) Depth of Permian rock map with a contour interval of 150 m. ♈ denoted the hot-springs.

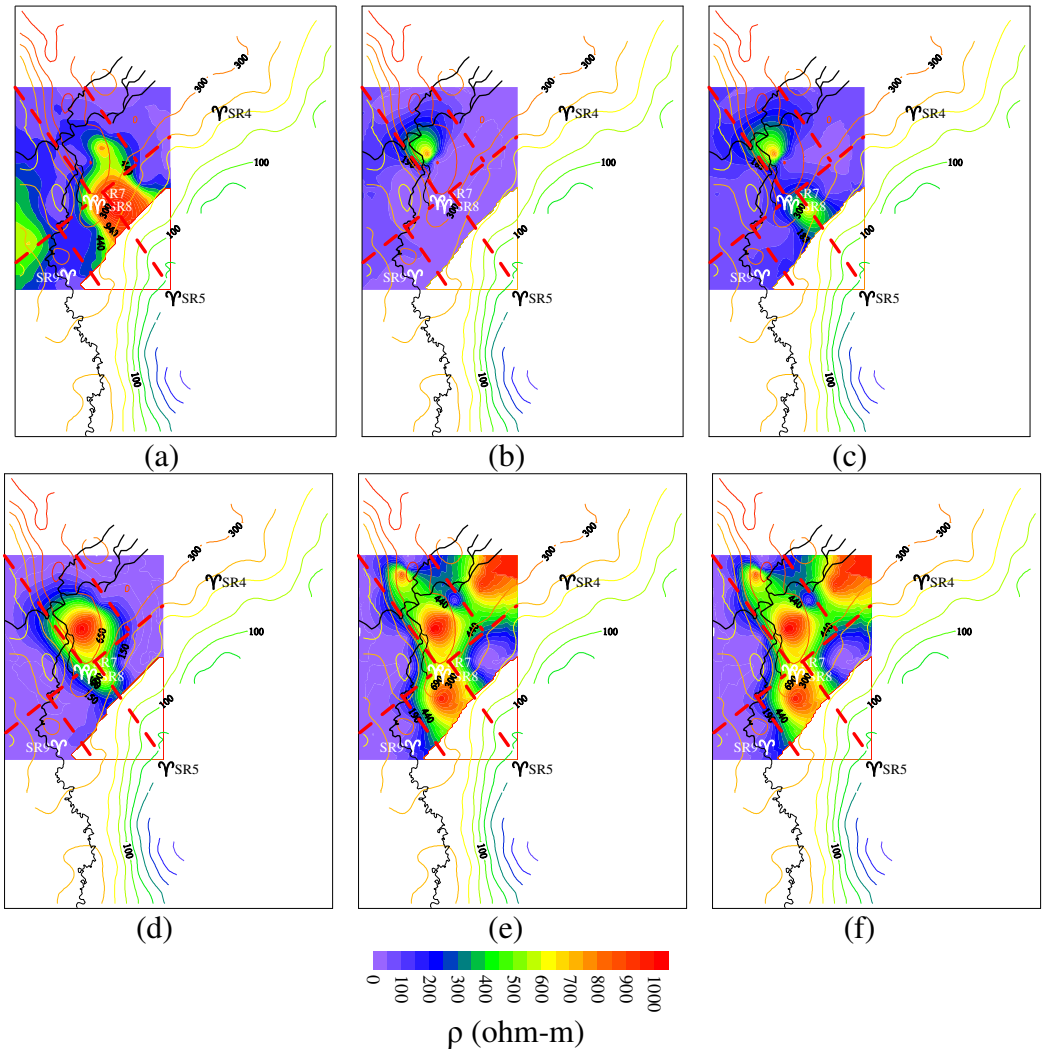

Figure 3.22 Bouguer anomaly and river course superimposed on contour maps of modeled resistivity at difference penetration depths around SR7 and SR8 hot-spring, at depths of; (a) 1.5 m., (b) 50 m., (c) 100 m., (d) 150 m., (e) 200 m., and (f) 250 m. ♈ denoted the hot-springs. The solid lines in black color and dash lines in red color are river and faults respectively.

3.4.6 Comparisons between resistivity model and gravity model

The resistivity models obtained from electric sounding were compared with interpreted geological cross-sections obtained from gravity model at shallow depth along 4 parallel lines, namely; JJ', KK', LL' and MM', as shown in Figure 3.23. The locations of those profiles are shown in Figure 3.16 (b). In these profiles, dashed lines represent the interfaces between Quaternary sediment and Triassic rocks and solid lines represent the interfaces between Triassic rocks and Permian limestone.

Along line JJ', a resistive bottom layer, 672 to 995 ohm-m at depths 75 to 280 m, was observed at four sounding points (S15, S16, S17, and S18) on the eastern part of the profile (Figure 3.23 (a)). It can be observed that two hot springs (SR7, SR8) are in the area of this resistive layer. They are close to the sounding point S16 of which resistive layer, 672 ohm-m, is determined at 75 m depth. This resistive layer is overlain by a low resistivity layer, 11 to 46 ohm-m, which is about 245 m thick on the eastern part of the profile and is very thick on the western part of the profile. The low and high resistivity layers correspond with layers of Quaternary sediment and Triassic rocks respectively on the gravity model.

Along line KK', a resistive bottom layer, 850 to 1,079 ohm-m at depths 118 to 137 m, was observed at two sounding points (S03 and S04) on the eastern part of the profile (Figure 3.23 (b)). It can be observed that two hot springs (SR7, SR8) are in the area of this resistive layer and are close to sounding point S03. This resistive layer is overlain by a low resistivity layer, 13 to 23 ohm-m, which is about 130 m thick on the eastern part of the profile and it is very thick on the western part of the profile. The depth to this high resistivity layer at sounding points S03 and S04 is approximately the same as the depth to interface between Triassic rocks and Permian limestone.

Along line LL', a resistive bottom layer, 801 to 959 ohm-m at depths 30 to 161 m, was observed at two sounding points, S12 in the middle part of the line and S10 on the eastern part of the profile (Figure 3.23 (c)). This resistive bottom layer is overlain a low resistivity layer, 7 to 63 ohm-m, which is about 160 m thick on the eastern end, 236 m on the western end, and is very thin in the middle part of the profile. The depth to this high resistivity layer at sounding points S12 and S10 is approximately close to the depth of interface between Triassic rocks and Permian limestone.

Along line MM', a resistive bottom layer, 912 ohm-m at 186 m depth, was observed at a sounding point, S21 on the eastern part of the profile (Figure 3.23 (d)). This resistive layer is overlain by a low resistivity layer, 11 to 34 Ohm-m, which is about 180 m thick on the eastern part of the profile and is very thick on the western part of the profile. The depth to this high resistivity layer at sounding points S21 is

approximately close to the depth of interface between Triassic rocks and Permian limestone.

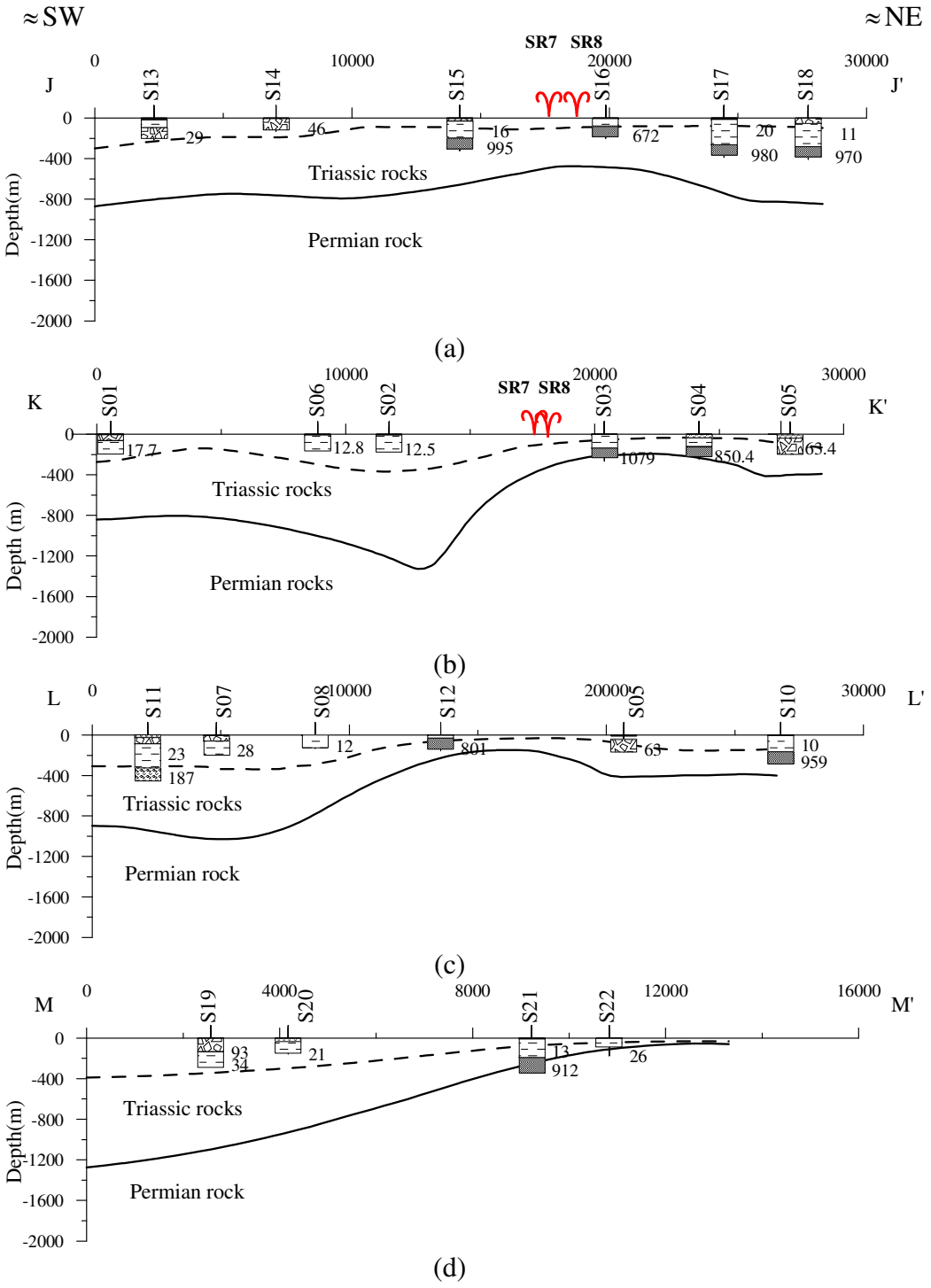

Figure 3.23 Resistivity and gravity models along the profiles (a) JJ′, (b) KK′, (c) LL′, and (d) MM′. Values in ohm-m. ♈ denoted the hot springs

3.4.7 Schematic geological cross-section of the study area

Schematic geological cross-section of the study area along the east-west profile obtained from the present study is shown in Figure 3.24. The horst and graben structures are pronounced in this study area. This horst and graben structures is probably the west extension of those developed in the Gulf of Thailand, east of the present study (Polachan and Sattayarak, 1989). It can be observed that hotsprings SR7 and SR8 are on the horst structure where Permian rock was uplifted. Therefore, fractures and fissures in Permian rocks and normal faults which bounded the horst structure may play roles as conduits or pathways of hot water. In addition, Permian rock is thought to be hot water reservoir of the geothermal system in the study area.

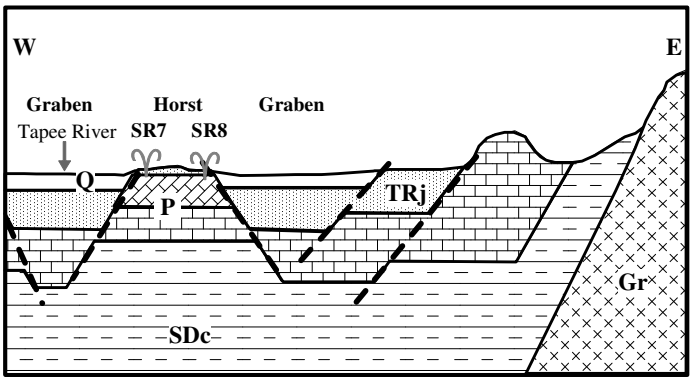

Figure 3.24 The schematic cross-section of the study area along east-west profile.